

# 2D or 3D: Who Governs Saliency in VLA Models? – Tri-Stage Token Pruning Framework with Modality Saliency Awareness

Zihao Zheng<sup>1</sup>, Sicheng Tian<sup>3</sup>, Zhihao Mao<sup>4</sup>, Lingyue Zhang<sup>5</sup>, Chenyue Li<sup>1</sup>, Ziyun Zhang<sup>1</sup>, Hong Gao<sup>2</sup>, Yuchen Huang<sup>2</sup>, Yutong Xu<sup>2</sup>, Guojie Luo<sup>1</sup>, †Xiang Chen<sup>1</sup>

<sup>1</sup> School of Computer Science, Peking University

<sup>2</sup> ZTE Corporation

<sup>3</sup> School of Artificial Intelligence, Beijing Normal University

<sup>4</sup> School of Computer Science, China University of Geosciences (Wuhan)

<sup>5</sup> School of Electronics Engineering and Computer Science, Peking University

## Abstract

Vision-Language-Action (VLA) models have emerged as the mainstream of embodied intelligence. Recent VLA models have expanded their input modalities from 2D-only to 2D+3D paradigms, forming multi-visual-modal VLA (MVLA) models. Despite achieving improved spatial perception, MVLA faces a greater acceleration demand due to the increased number of input tokens caused by modal expansion. Token pruning is an effective optimization method tailored to MVLA models. However, existing token pruning schemes are designed for 2D-only VLA models, ignoring 2D/3D modality saliency differences. In this paper, we follow the application process of multi-modal data in MVLA models and develop a tri-stage analysis to capture the discrepancy and dynamics of 2D/3D modality saliency. Based on these, we propose a corresponding tri-stage token pruning framework for MVLA models to achieve optimal 2D/3D token selection and efficient pruning. Experiments show that our framework achieves up to a 2.55× inference speedup with minimal accuracy loss, while only costing 5.8% overhead. Our Code is coming soon.

## 1 Introduction

Vision-Language-Action (VLA) models have emerged as the mainstream paradigm for embodied intelligence, achieving remarkable performance [3, 8, 15]. These models integrate visual encoders, Large Language Models (LLMs), and action decoders into a unified architecture [8, 46]. During the generation process, VLA models employ language instructions and visual observations as multi-modal inputs, and directly output precise robot control signals [2, 38].

Early VLA models utilize only 2D images as the visual input modality [3, 15]. While this design enables basic action generation, pure 2D visual representations insufficiently encode environmental spatial attributes and structures in complex scenarios and long-horizon tasks [8, 39]. To purchase better performance, researchers and industries extend the modalities of VLA models by integrating 3D visual information [9, 17]. 3D modalities (e.g. 3D point cloud) contain more spatial information [22, 27, 29], which can improve VLAs’ spatial perception and complex manipulation capabilities [16, 21]. For brevity, 2D-only VLA models are referred to as **single-visual-modal VLAs (SVLAs)** in this paper, while those 2D+3D VLA models are termed **multi-visual-modal VLAs (MVLAs)**.

After modal expansion, the data utilization paradigm of MVLA Models becomes complex. Fig. 1 (a) shows the whole process, which

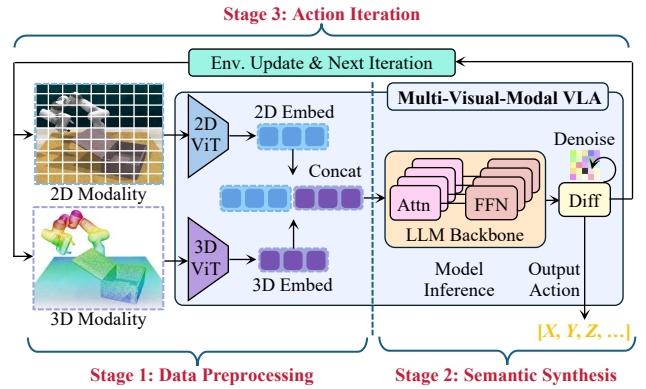


Figure 1: Data Utilization Paradigm in MVLA Inference

can be divided into three stages [17, 32]. In data preprocessing stage, 2D and 3D data are encoded via their respective ViT encoders [7, 16] and subsequently concatenated. In semantic synthesis stage, the LLM backbone conducts reasoning based on multi-modal semantics and employs a diffusion-based model to generate actions [19, 39]. In action iteration stage, the environment is updated after action execution, and the above process is iteratively repeated to form an action sequence [3, 15].

These complex data utilization paradigms incur substantial computational overhead, which constitutes a key bottleneck limiting the practical application of MVLA models. Without specific optimization, they can only produce actions at 3~5 Hz, well below the real-time requirement of approximately 20~30 Hz [23]. Numerous studies have explored inference optimization and deployment acceleration for VLA models, encompassing architecture redesign [5, 26], model compression [34, 41], decoding optimization [31, 42, 43], runtime acceleration [33, 44] and edge-cloud deployment [40, 45]. These methods effectively accelerate VLA inference and lay a foundation for the real-time application.

When facing novel MVLA models, the aforementioned methods fail to deliver satisfactory acceleration, as they are designed for SVLA models and ignore a key factor: **input tokens**. The extension of MVLA models to 3D modalities leads a rapid increase in input tokens, which is the primary reason for its higher computation overhead compared to SVLA models [39]. For instance, the latest MLA model [21] uses 256 tokens for 2D feature capture; after integrating 3D modalities, an additional 256 tokens are employed for

† Corresponding Author.

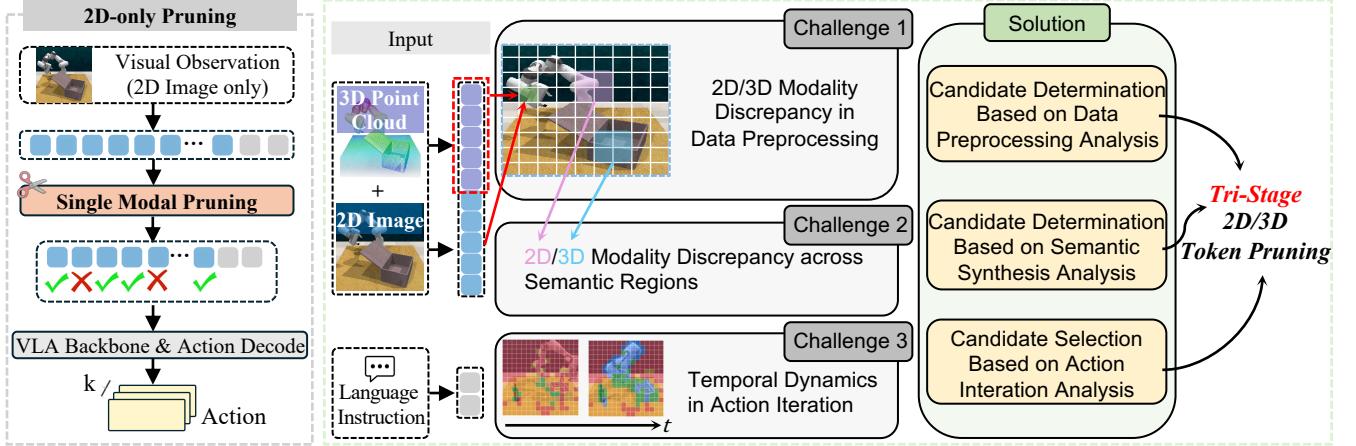


Figure 2: Comparison of Existing SVLA Token Pruning and Our Tri-Stage MVLA Token Pruning

3D feature capture. Therefore, token pruning, a method for inference acceleration by reducing redundant tokens (especially visual tokens), exhibits greater potential in MVLA optimization.

However, although some studies have successfully integrated dynamic/static token pruning strategies into SVLA models [18, 20], these approaches cannot be directly applied to MVLA models as they ignore modality salience (Fig. 2). **1) In the data preprocessing stage**, integrating 3D modalities introduces 2D/3D modal salience discrepancies, which cause inconsistent contributions of different modalities to the model. **2) In the semantic synthesis stage**, 2D/3D modal salience discrepancies are further influenced within distinct semantic patches and vary with semantics, leading to cross-semantic salience differences. **3) In the action iteration stage**, 2D/3D modal salience discrepancies fluctuate with progress and environmental variations during the iteration process. Existing pruning methods fail to quantify these discrepancies/dynamics of modality salience across three stages, leading to design mismatches and suboptimal performance when applied to MVLA models.

To address these, we conduct a tri-stage analysis (corresponding to the three stages as Fig. 1 shown) for MVLA models to revealing the discrepancies/dynamics of 2D/3D modality salience. Specifically, in the data preprocessing stage, we leverage model output features to reflect 2D/3D modality salience and propose a quantitative representation method for such salience based on feature norms. Furthermore, in the semantic synthesis stage, we use attention scores to reveal this modality salience across different semantic patch sets and put forward a salience decomposition mechanism. Finally, in the action iteration stage, based on the above analysis, we further reveal the dynamic fluctuation of 2D/3D modality salience during continuous action iterations.

Based on analysis results, we further propose a tri-stage token pruning framework. Specifically, in the data preprocessing stage, we utilize 2D/3D modality to set two thresholds for pruning candidate determination. In the semantic synthesis stage, we partition patches into semantic sets and adaptively configure pruning candidate sets for 2D/3D modalities within each semantic set. In the action iteration stage, we propose a temporal segmentation and salience

prediction mechanism to capture their dynamics for adaptive pruning adjustments. Finally, we fuse these tri-stage mechanisms to achieve efficient token pruning for MVLA models.

In summary, our contributions are as follows:

- We propose a tri-stage analysis to reveal the discrepancies and dynamics of 2D/3D modality salience, and identify when and which modality governs salience in MVLA models.
- Based on these analyses, we develop a tri-stage token pruning framework for MVLA models, which automatically selects optimal pruning configurations and enables efficient pruning.
- We conduct sufficient simulation and real-world experiments to verify the effectiveness and correctness of our framework, discuss its overhead, and outline future applications.

Experiment results show that, compared to Sort-of-the-Art (SOTA) baselines, our framework achieves  $2.55\times$  speedup with minimal accuracy loss, while only cost 5.8% overhead. We believe the proposed analysis and token pruning framework will support future VLA optimization and their modal expansion.

## 2 Background

### 2.1 VLA Models

**2.1.1 Architecture of VLA Models.** VLA models consist of three components: visual encoders for environment perception, LLM backbone for reasoning, and action decoders for action predict [2, 38]. Early VLA models use de-tokenizers as action decoders [3, 15]. With technology advances, SOTA VLA models adopt diffusion-based models as action decoders for direct generation [19, 32].

**2.1.2 Modality Expansion of VLA Models.** Early VLA models usually use 2D images as visual inputs (termed single-visual-modal VLA, SVLA) [3, 4, 15]. With developments, SOTA VLA models have integrated 3D visual modalities (e.g., 3D point clouds) to improve task success rate [21, 39], referred to as multi-visual-modal VLA (MVLA). However, this expansion of modalities notably increases the number of input tokens, which substantially elevates computational overhead and inference latency.

**2.1.3 Data Utilization Paradigm in MVLA Inference.** After modality expansion, the data utilization paradigm of MVLA Models

**Table 1: Analysis Results of Data Preprocessing Stage**

Env. &	Task	w/o Prune	Case Study 1: w/ Naive Prune				Case Study 2: w/ Naive Prune				Case Study 3: w/ Naive Prune			
Model	Description	SR	SR@2D( $r=50\%$ )	SR@3D( $r=50\%$ )	$M_{2D}^{S1}$	$M_{3D}^{S1}$	SR@2D( $r=50\%$ )	SR@3D( $r=50\%$ )	$M_{2D}^{S1}$	$M_{3D}^{S1}$	SR@2D( $r=50\%$ )	SR@3D( $r=50\%$ )	$M_{2D}^{S1}$	$M_{3D}^{S1}$
MLA [21]	Close Box	55.00%	6.67%	↓46.66%	40.00%	↓13.33%	90.16%	9.84%	45.00%	↓10.00%	70.00%	↑23.33%	90.31%	9.69%
	Close Fridge	56.66%	33.33%	↓23.33%	70.00%	↑13.34%	81.47%	18.53%	50.00%	↓6.66%	40.00%	↓16.66%	88.24%	11.76%
	Close Laptop	80.00%	53.33%	↓13.34%	90.00%	↑23.33%	90.38%	9.62%	90.00%	↑13.34%	80.00%	–	91.48%	8.52%
RLBench [12]	Swee Dustpan	66.67%	43.33%	↓23.34%	96.67%	↑30.00%	89.40%	10.60%	53.33%	↓13.34%	70.00%	↑3.33%	90.27%	9.73%
	Phone on Base	40.00%	35.00%	↓5.00%	53.33%	↑13.33%	90.43%	9.57%	33.33%	↓6.67%	55.00%	↑15.00%	90.12%	9.88%

becomes complex. As shown in Fig. 1, the whole process can be divided into three stages: data pre-processing stage, semantic synthesis stage and action iteration stage. These three phases provide a blueprint for our analysis and design.

## 2.2 Token Pruning

**2.2.1 Conventional Token Pruning.** Token pruning is a prevalent inference optimization method, derived from the observation that tokens in input sequences exhibit unequal saliency [10, 25]. With the emergence of LLMs, token pruning methods have been extensively developed to identify the static or dynamic redundancy of input tokens during inference, thus reducing computational overhead [13, 37]. Following the application of Vision-Language Models (VLMs), token pruning has become increasingly popular, driven by the high redundancy in visual tokens [6, 35].

**2.2.2 Token Pruning for SVLA Models.** Some studies have adapted token pruning methods to SVLA models. Early adaptations initially rely on static heuristics, using semantic saliency together with spatial and temporal redundancy to filter out unimportant tokens [20, 28]. To further preserve action-critical features, subsequent approaches incorporate task alignment to selectively retain only tokens highly correlated with instructions or manipulation targets [24, 30]. Current efforts advance dynamic, end-to-end adaptive mechanisms, such as differentiable dropping and diversity-aware selection, to optimize the trade-off between computational overhead and control precision [14, 18, 36]. Overall, these works effectively accelerate the inference of SVLA models with minimal performance degradation.

**2.2.3 Token Pruning for MVLA Models.** However, existing token pruning methods tailored for SVLA models are no longer optimal for MVLA models, as they overlook the saliency of 2D/3D modalities. The saliency of 2D/3D modalities varies across all three stages of data application paradigms and exhibits temporal dynamics in the execution process of complex embodied tasks. A detailed analysis and real-time capture of 2D/3D modal saliency, followed by its application to token pruning, constitutes the core for achieving the optimal Pareto frontier.

## 3 Tri-Stage Modality Saliency Analysis

In this section, we conduct comprehensive analyses of 2D/3D modalities across three stages: the data preprocessing, the semantic synthesis, and the action iteration. Based on the above analysis results, we derive key insights for implementing adaptive token pruning.

### 3.1 Analysis of Data Preprocessing Stage

*Motivation ①:* After modal expansion, discrepancies in 2D/3D modality saliency during the data preprocessing stage remain unclear and hard to quantify, which constrain token pruning designs.

#### 3.1.1 2D/3D Modality Saliency in Data Preprocessing Stage.

In MVLA models, the integration of 3D tokens significantly extends the inference sequence length (Sec. 2.1.2), which is the primary cause of MVLA’s slower inference speed than SVLA. It is intuitive that 2D and 3D information both act as descriptive representations of environments and objects, yet the information they convey exhibits significant differences for models, i.e. regarding which modality contributes more to the model. We design simple case studies to systematically explore this. Specifically, we select the recent SOTA work MLA [21] as test MVLA model. This model fuses multi-modal inputs, including 2D RGB images and 3D point clouds. We evaluate on five representative tasks in the RLBench [12] simulation environment and report task success rate (SR). Each task consists of 30 trials. During evaluation, a naive token pruning strategy is implemented to explore modality saliency: random pruning is performed at a ratio of  $r$  ( $r = 50\%, 60\%, 70\%$ ), targeting either only 2D-related tokens (represented as ‘@2D’) or only 3D-related tokens (represented as ‘@3D’).

Tab. 1 shows the results of these case studies. Most of the tasks exhibit a pattern where the success rate generally decreases in the only-2D prune scenario, while it generally increases in the only-3D prune scenario. Moreover, the SR degradation caused by only-3D pruning is significantly less than that induced by only-2D pruning. Taking the Close Box task as an example, in Case Study 1 ( $r=50\%$ ), the SR degradation induced by 3D-only pruning is 13.33%, whereas that induced by 2D-only pruning reaches 46.66%. Notably, some tasks exhibit increased accuracy after pruning. This is presumably because random pruning eliminates redundant information that interferes with model judgment, thereby facilitating the model’s environmental perception and intelligent reasoning. Moreover, we find that such special scenarios are more common when only-3D pruning is performed. Overall, our case studies demonstrate that 2D and 3D modalities exhibit distinct saliency and differ in their contributions to the model, with 2D modality showing significantly higher saliency than 3D modality.

#### 3.1.2 2D/3D Modality Saliency Representation in Data Preprocessing Stage.

After reaching the above conclusions, a key question is how to quantify modal saliency to enable its role in token pruning design. Fortunately, we propose a decomposition mechanism to address this issue. Specifically, 2D/3D data ultimately acts on the model, meaning the saliency to be evaluated originates from the model; thus, the features of the model’s final layer (`lm_head`) are selected for quantified representation. We first hook the output

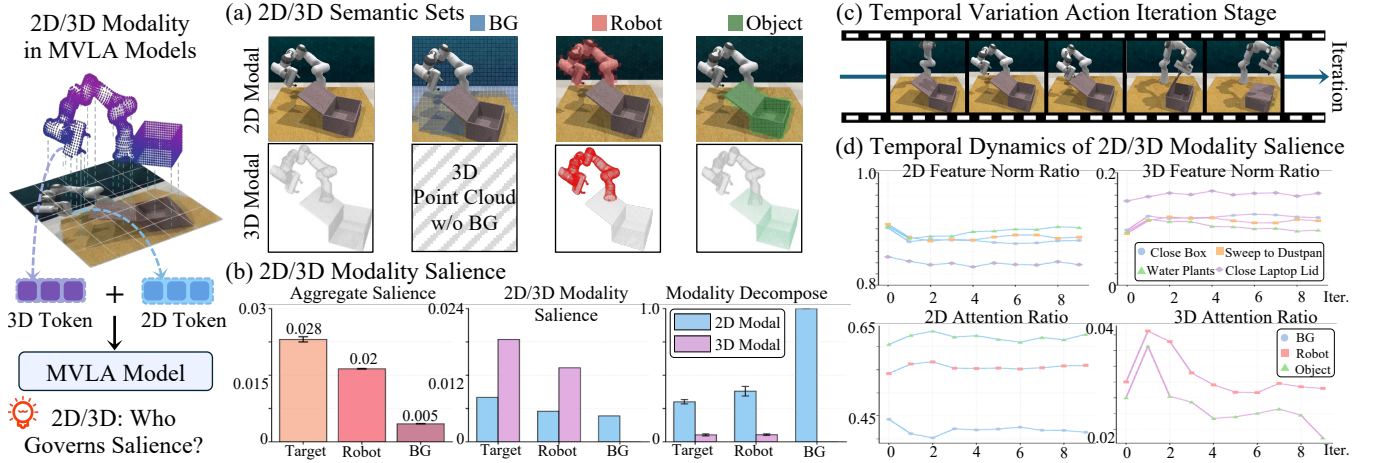


Figure 3: (a) Analysis of Semantic Synthesis Stage (b) Analysis of Action Iteration Stage

feature of final layer. Furthermore, we determine which features in the feature set originate from 2D and which from 3D based on the token sequence, noted as  $f_{2D}$  and  $f_{3D}$  respectively. After that, for each visual patch  $p$ , we compute the  $L_1$  norm ( $\|\cdot\|_1$ ) of  $f_{2D}$  and  $f_{3D}$ , serving as a quantified representation of modality saliency. Then, we calculate the saliency percent (noted as  $\mathcal{M}$ ) of  $\|f_{2D}\|_1^p$  and  $\|f_{3D}\|_1^p$ , as shown in Eq. (1). In Eq. (1), S1 means stage 1 (data preprocessing) and  $\psi$  means the state observer.

$$\mathcal{M}_{\text{modal}}^{S1} = \text{avg} \left( \sum_p \frac{\|f_{\text{modal}}\|_1^p}{\|f_{2D}\|_1^p + \|f_{3D}\|_1^p}; \text{modal} \in \{2D, 3D\}; p \in \psi \right). \quad (1)$$

We calculate  $\mathcal{M}_{S1}$  on aforementioned tasks, and showcase the results of  $\mathcal{M}_{S1}$  in Tab. 1. As shown in Tab.1, on all five tasks,  $\mathcal{M}_{2D}^{S1}$  are much higher than  $\mathcal{M}_{3D}^{S1}$ . Therefore, we not only demonstrate that the 2D modality is more important in Stage 1, but also quantify the saliency of the 2D and 3D modalities respectively.

**Insight ①: Leveraging model features, the proposed metric  $\mathcal{M}_{\text{modal}}^{S1}$  captures modal saliency and supports the design of token pruning.**

## 3.2 Analysis of Semantic Synthesis Stage

*Motivation ②: Although the 2D/3D modality saliency in the data processing stage can be quantified, such saliency is further integrated into semantic sets during the subsequent semantic synthesis stage.*

### 3.2.1 2D/3D Modality Saliency in Semantic Synthesis Stage.

From this motivation, it is necessary to further analyze the discrepancies in 2D/3D modality saliency specifically for the semantic synthesis stage. To achieve this, we first need to formulate the semantic sets. Based on the conclusions of existing studies (e.g., VLA-Cache [33] and Oat-VLA [1]), VLA models primarily encompass three core semantic components: background (noted as  $\mathcal{S}_{2D}^{\text{bg}}$ ), robot main body (noted as  $\mathcal{S}_{2D}^{\text{rob}}$  and  $\mathcal{S}_{3D}^{\text{rob}}$ ), and the target object (noted as  $\mathcal{S}_{2D}^{\text{obj}}$  and  $\mathcal{S}_{3D}^{\text{obj}}$ ). 3D modality lacks background information and thus do not possess corresponding semantic sets. We adopt this conclusion and use these three semantic sets as the basis for further analyzing 2D/3D modality saliency in the semantic synthesis stage.

Next, we need to explore how to accurately partition complex 2D/3D patches into three semantic sets. To achieve this, we select the attention scores (noted as  $\alpha$ ) that are most semantically relevant. Specifically, we first partition the attention matrix according to the modality of tokens to obtain attention submatrices representing the 2D and 3D modalities. Then, we cluster the submatrices. The cluster centers for 2D modality are set to 3 (corresponding to  $\mathcal{S}_{2D}^{\text{bg}}$ ,  $\mathcal{S}_{2D}^{\text{rob}}$ , and  $\mathcal{S}_{2D}^{\text{obj}}$ ). The cluster centers of the 3D modality are set to 2 (corresponding to  $\mathcal{S}_{3D}^{\text{bg}}$ ,  $\mathcal{S}_{3D}^{\text{rob}}$ , and  $\mathcal{S}_{3D}^{\text{obj}}$ ). Correspondences between semantic sets and clustering results are then established, with the findings presented in Fig. 3 (a). The results in Fig. 3 (a) confirm the correctness of our clustering, which can assign semantics to each clustering result with negligible bias.

$$\mathcal{S}_{\text{total}}^{\text{Sem}} = \mathcal{S}_{2D}^{\text{Sem}} + \mathcal{S}_{3D}^{\text{Sem}}, \text{Sem} \in \{\text{bg, rob, obj}\}. \quad (2)$$

$$\alpha_{\text{Sem}} = \text{avg} \left( \sum_p (\|\alpha_{2D}^{\text{Sem}}\|_1 + \|\alpha_{3D}^{\text{Sem}}\|_1) \right), \text{Sem} \in \{\text{bg, rob, obj}\}. \quad (3)$$

Then, we aggregate the attention scores of all semantic sets, which are used as a semantic-level metric for 2D/3D modal saliency, as Eq. (3). The left panel of Fig. 3 (b) presents the aggregated results for three semantic sets, which indicate that  $\alpha_{\text{bg}} > \alpha_{\text{rob}} \gg \alpha_{\text{obj}}$ , suggesting a significant disparity in saliency across different semantic patches, particularly in the background regions.

### 3.2.2 2D/3D Modality Saliency Representation in Semantic Synthesis Stage.

Following the derivation of the above conclusions, it is necessary to address how to achieve quantitative representation of 2D/3D modal saliency during the semantic integration stage. Based on the findings from the data preprocessing stage, the 2D modality exhibits greater saliency than the 3D modality; thus, we decompose the attention scores of the 3D modality into those of the 2D modality. Specifically, for a given patch  $p$ ,  $\alpha_{2D}^{\text{Sem}}$  and  $\alpha_{3D}^{\text{Sem}}$  are all vectors, we decompose the  $\alpha_{3D}^{\text{Sem}}$  into  $\alpha_{2D}^{\text{Sem}}$ , as shown in Eq. (4).

$$\alpha_{3D}^{\text{Sem}} = \{\alpha_{3D}^{\text{Sem}}\}_{\text{para}} + \{\alpha_{3D}^{\text{Sem}}\}_{\text{ortho}} \quad (4)$$

In Eq. (4),  $\{\alpha_{3D}^{\text{Sem}}\}_{\text{para}}$  means the parallel part and  $\{\alpha_{3D}^{\text{Sem}}\}_{\text{ortho}}$  means the orthogonal part. After the decomposition is completed,  $\{\alpha_{3D}^{\text{Sem}}\}_{\text{para}}$  and  $\{\alpha_{3D}^{\text{Sem}}\}_{\text{ortho}}$  are all explainable.  $\{\alpha_{3D}^{\text{Sem}}\}_{\text{ortho}}$  denotes

the overlapping representation between 3D and 2D modalities, which can be considered redundant. While  $\{\alpha_{3D}^{\text{Sem}}\}_{\text{ortho}}$  denotes the fully orthogonal representation between 3D and 2D modalities, which can be regarded as the unique information of 3D. After that, we calculate their average percentage  $M_{2D}^{\text{S2}}$  and  $M_{3D}^{\text{S2}}$  as defined in Eq. (5) and Eq. (6). Note that ‘S2’ means stage 2 (i.e., semantic synthesis stage).

$$M_{2D}^{\text{S2}} = \text{avg} \left( \sum_p^{\text{Sem}} \frac{\|\alpha_{2D}^{\text{Sem}}\|_1}{\|\alpha_{2D}^{\text{Sem}}\|_1 + \|\alpha_{3D}^{\text{Sem}}\|_1} \right), \text{Sem} \in \{\mathcal{S}_{\text{bg}}, \mathcal{S}_{\text{rob}}, \mathcal{S}_{\text{obj}}\} \quad (5)$$

$$M_{3D}^{\text{S2}} = \text{avg} \left( \sum_p^{\text{Sem}} \frac{\|\{\alpha_{3D}^{\text{Sem}}\}_{\text{ortho}}\|_1}{\|\alpha_{2D}^{\text{Sem}}\|_1 + \|\alpha_{3D}^{\text{Sem}}\|_1} \right), \text{Sem} \in \{\mathcal{S}_{\text{bg}}, \mathcal{S}_{\text{rob}}, \mathcal{S}_{\text{obj}}\} \quad (6)$$

We have tested the proposed metric  $M_{2D}^{\text{S2}}$ , and the results are shown in Fig. 3(b) middle and right part. From the results, we find that in the target and robot patch sets, the saliency of the 3D modality is significantly higher than that of the 2D modality, even though in these two regions, the proportion of the 3D modality is lower than that of the 2D modality (as shown in the right part). To date, we achieve the quantitative characterization of 2D/3D modal saliency in the semantic synthesis stage, which facilitates the design of our token pruning strategy.

**Insight ②: The proposed  $M_{2D}^{\text{S2}}$  and  $M_{3D}^{\text{S2}}$  could capture the 2D/3D modality saliency discrepancy in semantic synthesis stage, which will support the token pruning designs.**

### 3.3 Analysis of Action Iteration Stage

*Motivation ③: During inference, MVLA models requires continuous environmental updates and action iterations; this process introduces temporal changes, leading to 2D/3D modality discrepancy variations.*  
**2D/3D Modality Saliency Dynamics in Action Iteration Stage.** Robotic manipulation is a highly dynamic process (like Fig. 3 (c)); consequently, across the execution timeline of a single task, neither the overall saliency of any given patch nor its reliance on the 2D and 3D modalities remains static. To systematically demonstrate this, we conduct experiments on the close\_box task in the RLbench simulation environment [11, 12, 21], evaluating 5 episodes with a maximum of 8 steps each. We continuously track the metric  $M_{2D}^{\text{S1}}(t)$  and  $M_{3D}^{\text{S1}}(t)$  that we proposed across different tasks, over the time step  $t$ . As shown in Fig. 3 (d), the two figures above illustrate that the saliency of 2D/3D modality changes at different stages of task execution, which need an effective prediction mechanism.

In parallel with the shift in data processing stage, the saliency of 2D/3D modality during semantic synthesis also undergoes dynamic evolution. Following the definitions in Sec. 3.2, we continuously track the metric  $M_{2D}^{\text{S2}}(t)$  and  $M_{3D}^{\text{S2}}(t)$  for distinct semantic regions across the early and late stages of the task. As shown in Fig. 3 (d), the attention allocated among the target, the robotic robot, and the background is continuously rebalanced throughout the entire manipulation trajectory. The dynamic nature of the action iteration provides a solid theoretical foundation for designing adaptive token pruning strategies tailored to different task phases.

**Insight ③: 2D/3D modality saliency will change with the action iteration, which means need a prediction mechanism to adaptive adjust pruning budget.**

### Algorithm 1 Tri-Stage Token Pruning Framework

---

**Input:** Current step  $t$ , Window size  $k$ , Observations  $X_t \in \{M_{2D,p}^{\text{S1}}, M_{3D,p}^{\text{S1}}, M_{2D,p}^{\text{S2}}, M_{3D,p}^{\text{S2}}\}$ , Attention weights  $\alpha$ , Momentum parameter  $\beta$ , Thresholds  $\tau_{2D}, \tau_{3D}$

**Init:** Candidate sets  $C^{\text{S1}} \leftarrow \emptyset, C^{\text{S2}} \leftarrow \emptyset, C_{\text{final}} \leftarrow \emptyset$ , Retention masks  $Mask_{2D} \leftarrow \emptyset, Mask_{3D} \leftarrow \emptyset$

**if**  $t == 1$  **then return** Full unpruned tokens (Cold Start Phase)

① **Action Iteration Stage:**

**for** each patch  $p$  and indicator  $X_t$  **do**

**if**  $1 < t < k$  **then**  $\hat{X}_t^{(p)} = \frac{t-1}{t} \hat{X}_{t-1}^{(p)} + \frac{1}{t} X_t^{(p)}$

**else**  $\hat{X}_t^{(p)} = \beta \cdot \hat{X}_{t-1}^{(p)} + (1 - \beta) \cdot X_t^{(p)}$

② **Data Preprocessing Stage:**

**for** each patch  $p$  **do**

**if**  $\hat{M}_{3D,p}^{\text{S1}} < \tau_{2D}$  **then**  $C_p^{\text{S1}} \leftarrow \{2D\}$

**else if**  $\hat{M}_{3D,p}^{\text{S1}} > \tau_{3D}$  **then**  $C_p^{\text{S1}} \leftarrow \{3D\}$

**else**  $C_p^{\text{S1}} \leftarrow \{2D, 3D\}$

③ **Semantic Synthesis Stage:**

Cluster  $\alpha \rightarrow \{\mathcal{S}_{\text{obj}}, \mathcal{S}_{\text{rob}}, \mathcal{S}_{\text{bg}}\}$  via 1D K-Means; Compute baselines  $\mu_{M_{2D}^{\text{S2}}}, \mu_{M_{3D}^{\text{S2}}}$

**for** each patch  $p$  **do**

**if**  $p \in \mathcal{S}_{\text{bg}}$  **then**  $C_p^{\text{S2}} \leftarrow \emptyset$  **if**  $\text{rand}() < 0.9$  **else**  $\{2D, 3D\}$

**else if**  $p \in \mathcal{S}_{\text{rob}}$  **then**

$C_p^{\text{S2}} \leftarrow \{2D, 3D\}$  **if**  $\hat{M}_{3D,p}^{\text{S2}} > \mu_{M_{3D}^{\text{S2}}}$  **else** ( $\{2D\}$  **if**  $\hat{M}_{2D,p}^{\text{S2}} > \mu_{M_{2D}^{\text{S2}}}$  **else**  $\emptyset$ )

**else** //  $p \in \mathcal{S}_{\text{obj}}$

$C_p^{\text{S2}} \leftarrow \{2D\}$  **if** ( $\hat{M}_{2D,p}^{\text{S2}} \gg 0 \wedge \hat{M}_{3D,p}^{\text{S2}} \rightarrow 0$ ) **else**  $\{2D, 3D\}$

④ **Overall Candidate Fusion:**

**for** each patch  $p$  **do**

**if**  $C_p^{\text{S2}} \neq \emptyset$  **then**

$C_{\text{final},p} = C_p^{\text{S2}} \cap C_p^{\text{S1}}$

**if**  $C_{\text{final},p} == \emptyset$  **then**  $C_{\text{final},p} \leftarrow C_p^{\text{S2}}$  // Conflict resolution

$Mask_{2D}^p = 1$  **if**  $2D \in C_{\text{final},p}$  **else**  $0$

$Mask_{3D}^p = 1$  **if**  $3D \in C_{\text{final},p}$  **else**  $0$

**return**  $Mask_{2D}, Mask_{3D}$  to network encoder

---

## 4 Tri-Stage Token Pruning Framework

Building on the insights from Sec. 3, we propose a tri-stage token pruning framework tailored to seamlessly integrate adaptive strategies across the MVLA inference pipeline.

### 4.1 2D/3D Pruning Candidate Determination Based on Data Preprocessing Analysis

Guided by Insight ① from Sec. 3.1.2, our data processing strategy dynamically exploits 2D/3D saliency differences during inference. Since a smaller feature norm indicates lower model dependence (Sec. 3.1.2), we evaluate the modality preference for a given patch  $p$  using its 3D feature proportion  $M_{3D}^{\text{S1}}$ . We map this continuous proportion to a discrete retention candidate set,  $C_p^{\text{S1}}$ , via a dual-threshold mechanism. Specifically, a lower bound  $\tau_{2D}$  and an upper bound  $\tau_{3D}$  partition the preference into three states. When  $M_{3D}^{\text{S1}} < \tau_{2D}$ , the 2D modality dominates (e.g., pure texture regions), rendering 3D features redundant and setting  $C_p^{\text{S1}} = \{2D\}$ . Conversely,  $M_{3D}^{\text{S1}} > \tau_{3D}$  indicates a high reliance on 3D geometric features, isolating the 3D modality ( $C_p^{\text{S1}} = \{3D\}$ ). For intermediate values ( $\tau_{2D} \leq M_{3D}^{\text{S1}} \leq \tau_{3D}$ ), the modalities are balanced and complementary, necessitating dual retention ( $C_p^{\text{S1}} = \{2D, 3D\}$ ). The sensitivity of hyperparameters  $\tau_{2D}$  and  $\tau_{3D}$  is detailed in Sec. 5.

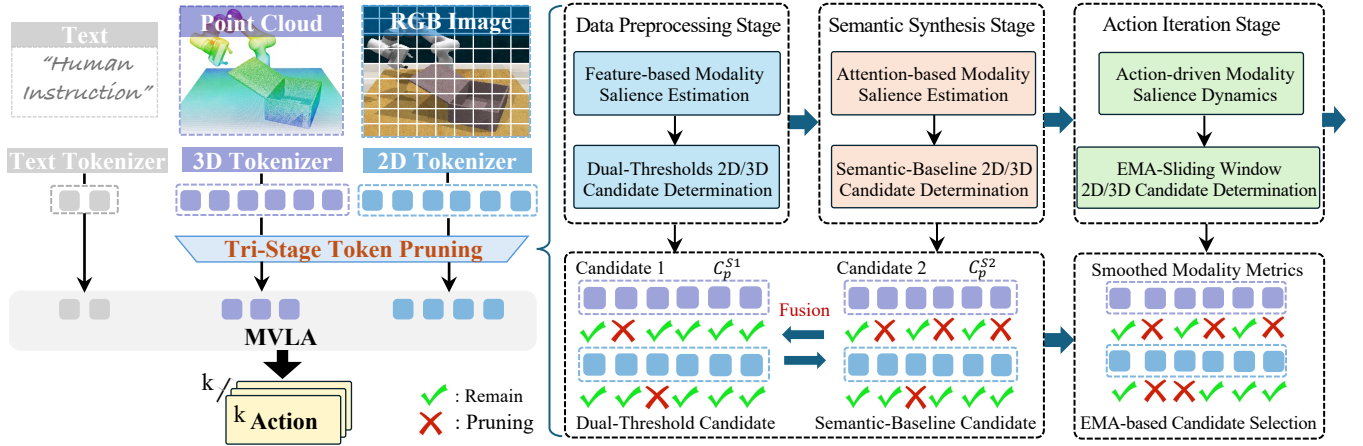


Figure 4: Tri-Stage Token Pruning Framework

## 4.2 2D/3D Pruning Candidate Determination Based on Semantic Synthesis Analysis

Guided by Insight ② from Sec. 3.2, our semantic synthesis strategy adaptively establishes pruning thresholds based on the global attention distribution and modality saliency within distinct semantic contexts. We first employ 1D K-Means ( $K=3$ ) on comprehensive attention scores to partition patches into the highly-responsive target object ( $\mathcal{S}_{obj}$ ), moderately-responsive robot arm ( $\mathcal{S}_{rob}$ ), and low-responsive background ( $\mathcal{S}_{bg}$ ). Concurrently, we compute global baseline thresholds for 2D ( $\mu_{M_{2D}^{S_2}}$ ) and pure 3D orthogonal ( $\mu_{M_{3D}^{S_2}}$ ) proportions using Eq. (5) and Eq. (6). These baselines strictly govern the dynamic semantic retention set,  $C_{S_2,p}$ . To efficiently maintain a weak global perception, background patches ( $p \in \mathcal{S}_{bg}$ ) undergo a 90% uniform random pruning, discarding the vast majority ( $C_p^{S_2} = \emptyset$ ). For robot arm patches ( $p \in \mathcal{S}_{rob}$ ), if pure 3D reliance exceeds the baseline ( $M_{3D}^{S_2} > \mu_{M_{3D}^{S_2}}$ )—indicating crucial spatial functions like collision avoidance—both modalities are retained ( $C_p^{S_2} = \{2D, 3D\}$ ). Conversely, regions dominant in 2D texture but below the 3D baseline ( $M_{3D}^{S_2} \leq \mu_{M_{3D}^{S_2}}$  and  $M_{2D}^{S_2} > \mu_{M_{2D}^{S_2}}$ ) are restricted to 2D retention ( $C_p^{S_2} = \{2D\}$ ). Finally, target object patches ( $p \in \mathcal{S}_{obj}$ ) default to dual-modality protection ( $C_p^{S_2} = \{2D, 3D\}$ ) for precise manipulation, degrading to single-modality retention ( $C_p^{S_2} = \{2D\}$ ) only when extreme 2D reliance and near-zero 3D responses render point cloud features strictly redundant.

## 4.3 2D/3D Pruning Candidate Selection Based on Action Iteration Analysis

Guided by the temporal dynamics observed during the action iteration stage (Sec. 3.3), our action iteration strategy leverages the temporal continuity between consecutive video frames to smooth pruning decisions. Instead of relying on instantaneous attention mutations, we introduce an Exponential Moving Average (EMA) mechanism based on a sliding window to incorporate prior historical information. For a given patch  $p$ , taking the 3D feature proportion  $M_{3D}^{S_1}$  (defined in Sec. 3.1) as an example, its temporally

smoothed prediction  $\hat{M}_{3D,p}^t$  at step  $t$  is calculated as:

$$\hat{M}_{3D,p}^t = \beta \cdot \hat{M}_{3D,p}^{t-1} + (1 - \beta) \cdot M_{3D,p}^t \quad (7)$$

where  $M_{3D,p}^{S_1,t}$  is the actual observation at the current frame, and  $\beta \in (0, 1)$  is the momentum parameter ensuring that the weight of historical information decays exponentially over time. Similarly, this EMA updating mechanism is synchronously applied to the attention proportions in the semantic dimension (defined in Sec. 3.2), predicting  $\hat{M}_{2D,p}^{S_1,t}$  and  $\hat{M}_{3D,p}^{S_1,t}$ . Ultimately, the threshold evaluations for both the modality and semantic dimensions strictly employ these temporally smoothed predictions. This approach effectively mitigates inter-frame flickering and enhances the robustness of modality retention decisions without incurring high overhead.

## 4.4 Overall Candidate Fusion

The ultimate objective of the tri-stage token pruning framework is to logically fuse the temporally smoothed semantic candidate set  $C_p^{S_2}$  and the modality candidate set  $C_p^{S_1}$ . We adopt a cascaded coarse-to-fine strategy—specifically, patch-level coarse pruning followed by modality-level fine separation—integrated with a temporal cold start mechanism to output the final token retention masks. To ensure decision stability, we propose an indicator  $X \in \{M_{2D,p}^{S_1}, M_{3D,p}^{S_1}, M_{2D,p}^{S_2}, M_{3D,p}^{S_2}\}$  used to generate the candidate sets strictly rely on sliding window predictions. During the initial phase of the video sequence, we implement a cold start mechanism to compute the predicted value  $\hat{X}_t$  at time step  $t$ . For the initial frame ( $t = 1$ ), which lacks historical information, we bypass EMA fitting to directly use the current observation ( $\hat{X}_1 = X_1$ ), performing no pruning to guarantee complete feature extraction. During the accumulation phase ( $1 < t < k$ ), where historical data is insufficient for a full window size  $k$ , we apply a dynamic EMA prediction formulated as shown in Eq. (8).

$$\hat{X}_t = \frac{t-1}{t} \hat{X}_{t-1} + \frac{1}{t} X_t. \quad (8)$$

Once the historical feature queue is full ( $t \geq k$ ), the standard EMA update is applied using a fixed momentum parameter  $\beta$  to

**Table 2: Results about Representative Tasks in RLbench Simulation Benchmark**

Methods	Close Box			Close Laptop			Close Fridge			Take Umbrella			Average		
	SR	Speed	2D/3D PR	SR	Speed	2D/3D PR	SR	Speed	2D/3D PR	SR	Speed	2D/3D PR	SR	Speed	2D/3D PR
MLA <sup>†</sup> [21] w/o pruning	55.0%	1.00×	0.0% / 0.0%	80.0%	1.00×	0.0% / 0.0%	35.0%	1.00×	0.0% / 0.0%	25.0%	1.00×	0.0% / 0.0%	48.8%	1.00×	0.0% / 0.0%
Naive Prune <sup>‡</sup> ( $r=50\%$ )	16.7%	1.22×	50.0% / 50.0%	33.3%	1.22×	50.0% / 50.0%	10.0%	1.22×	50.0% / 50.0%	6.7%	1.22×	50.0% / 50.0%	14.2%	1.22×	50.0% / 50.0%
Naive Prune <sup>‡</sup> ( $r=60\%$ )	23.3%	1.39×	60.2% / 60.2%	46.7%	1.39×	60.2% / 60.2%	16.7%	1.39×	60.2% / 60.2%	10.0%	1.39×	60.2% / 60.2%	24.2%	1.39×	60.2% / 60.2%
Naive Prune <sup>‡</sup> ( $r=70\%$ )	13.3%	1.47×	69.9% / 69.9%	43.3%	1.47×	69.9% / 69.9%	6.7%	1.47×	69.9% / 69.9%	3.3%	1.47×	69.9% / 69.9%	16.7%	1.47×	69.9% / 69.9%
Naive Prune <sup>‡</sup> ( $r=80\%$ )	13.3%	1.57×	80.1% / 80.1%	30.0%	1.57×	80.1% / 80.1%	3.3%	1.57×	80.1% / 80.1%	0.0%	1.57×	80.1% / 80.1%	11.7%	1.57×	80.1% / 80.1%
SP-VLA [18] ( $r=50\%$ )	13.3%	1.21×	33.7% / 61.3%	16.7%	1.22×	35.7% / 61.3%	10.0%	1.21×	34.2% / 61.3%	3.3%	1.22×	35.4% / 61.3%	10.8%	1.22×	34.8% / 61.3%
SP-VLA [18] ( $r=60\%$ )	16.7%	1.37×	39.3% / 76.6%	43.3%	1.39×	46.1% / 76.6%	20.0%	1.38×	42.8% / 76.6%	6.7%	1.38×	43.9% / 76.6%	21.7%	1.38×	43.0% / 76.6%
SP-VLA [18] ( $r=70\%$ )	10.0%	1.43×	43.1% / 89.1%	46.7%	1.47×	49.5% / 89.1%	6.7%	1.44×	46.3% / 89.1%	3.3%	1.45×	47.8% / 89.1%	16.7%	1.45×	46.7% / 89.1%
SP-VLA [18] ( $r=80\%$ )	13.3%	1.45×	43.0% / 93.4%	33.3%	1.46×	44.2% / 93.4%	3.3%	1.45×	43.2% / 93.4%	0.0%	1.46×	43.8% / 93.4%	12.5%	1.46×	43.6% / 93.4%
VLA-Pruner [20] ( $r=50\%$ )	20.0%	1.22×	50.0% / 50.0%	43.3%	1.22×	50.0% / 50.0%	16.7%	1.22×	50.0% / 50.0%	10.0%	1.22×	50.0% / 50.0%	22.5%	1.22×	50.0% / 50.0%
VLA-Pruner [20] ( $r=60\%$ )	16.7%	1.39×	60.2% / 60.2%	53.3%	1.38×	60.2% / 60.2%	20.0%	1.38×	60.2% / 60.2%	13.3%	1.39×	60.2% / 60.2%	25.8%	1.39×	60.2% / 60.2%
VLA-Pruner [20] ( $r=70\%$ )	16.7%	1.49×	69.9% / 69.9%	50.0%	1.48×	69.9% / 69.9%	13.3%	1.48×	69.9% / 69.9%	6.7%	1.49×	69.9% / 69.9%	21.7%	1.49×	69.9% / 69.9%
VLA-Pruner [20] ( $r=80\%$ )	33.3%	1.57×	80.1% / 80.1%	40.0%	1.56×	80.1% / 80.1%	10.0%	1.56×	80.1% / 80.1%	3.3%	1.57×	80.1% / 80.1%	21.7%	1.57×	80.1% / 80.1%
Ours ( $r=50\%$ )	70.0%	2.43×	37.4% / 62.8%	30.0%	2.55×	41.7% / 60.4%	60.0%	2.40×	34.4% / 40.0%	30.0%	2.59×	42.6% / 79.5%	47.5%	2.49×	39.0% / 60.7%
Ours ( $r=60\%$ )	60.0%	2.45×	45.1% / 72.8%	35.0%	2.55×	47.6% / 66.6%	55.0%	2.30×	32.7% / 42.7%	10.0%	2.63×	49.2% / 82.2%	40.0%	2.48×	43.6% / 66.1%
Ours ( $r=70\%$ )	50.0%	2.55×	58.0% / 78.2%	65.0%	2.44×	52.5% / 69.5%	45.0%	2.51×	49.1% / 63.9%	25.0%	2.69×	59.0% / 79.6%	46.3%	2.55×	54.7% / 72.8%
Ours ( $r=80\%$ )	40.0%	2.48×	56.3% / 76.6%	50.0%	2.61×	58.4% / 79.6%	50.0%	2.42×	49.1% / 66.6%	20.0%	2.53×	61.0% / 83.0%	40.0%	2.51×	56.2% / 76.4%

<sup>†</sup>PR' means pruning rate. <sup>‡</sup>MLA is the selected MVLA model; all baselines migrate their pruning strategies onto it. <sup>‡</sup>Naive Prune randomly prunes tokens with equal 2D/3D ratios.

smooth pruning decisions as shown in Eq. (9).

$$\hat{X}_t = \beta \cdot \hat{X}_{t-1} + (1 - \beta) \cdot X_t. \quad (9)$$

The candidate sets  $C_p^{S_2^2}$  and  $C_p^{S_1^1}$  for each patch  $p$  are then independently calculated based on these temporally smoothed predictions. Following candidate set generation, we conduct a patch-level coarse filtering in the spatial dimension to strip away irrelevant regions. Utilizing the semantic dimension’s output as a hard macro-spatial constraint, any patch  $p$  classified as an irrelevant background region (i.e.,  $C_p^{S_2^2} = \emptyset$  for  $p \in \mathcal{S}_{bg}$ ) is deemed to lack sufficient attention response and is directly discarded. The remaining patches ( $C_p^{S_2^2} \neq \emptyset$ ) are aggregated into a high-priority retention set  $\mathcal{P}_{active}$ . For these critical patches, single-modality redundancy may still exist internally; for instance, a robotic arm region ( $\mathcal{S}_{rob}$ ) might only necessitate 2D texture, whereas structural components might strictly rely on 3D geometry. To achieve precise modality-level separation, we perform an intersection fusion defined as  $C_p^{final} = C_p^{S_2^2} \cap C_p^{S_1^1}$ . This intersection logically ensures that only modalities satisfying both global semantic requirements (the upper bound) and sufficient local feature representation are preserved. In rare instances where the intersection is empty ( $C_p^{S_2^2} \cap C_p^{S_1^1} = \emptyset$ )—indicating that a globally required modality appears as noise in local features—we trigger a conflict resolution fallback that forces  $C_p^{final} = C_p^{S_2^2}$  to prevent feature disruption in critical regions. Based on  $C_p^{final}$ , we generate token retention masks for the dual-branch network as Eq. (10). Tokens assigned a mask value of 1 proceed to subsequent layer computations, while those with a value of 0 are discarded.

$$Mask_{2D}^p = \begin{cases} 1, & \text{if } 2D \in C_p^{final} \\ 0, & \text{otherwise.} \end{cases}, \quad Mask_{3D}^p = \begin{cases} 1, & \text{if } 3D \in C_p^{final} \\ 0, & \text{otherwise.} \end{cases} \quad (10)$$

## 5 Experiments

### 5.1 Setup

We instantiate tri-stage token pruning on MLA [21] from its open-sourced post-trained checkpoint, modifying only the pruning strategy while keeping the underlying policy unchanged. The 2D stream

produces 256 image tokens ( $16 \times 16$  patches) and the point encoder generates 256 point tokens prior to pruning. We evaluate on the RLbench simulator [11, 12] and report task success rate (SR) and end-to-end speedup. We compare five settings: unpruned MLA, Naive Prune (random), SP-VLA [18], VLA-Pruner [20], and our method. All are implemented on the same MLA backbone under identical task settings. All experiments run on a single NVIDIA A100-PCIE-40GB GPU with an Intel Xeon Gold 6348 CPU.

## 5.2 Main Results

**5.2.1 Results on Simulation Benchmarks.** We evaluate our tri-stage token pruning framework and all baselines across four representative RLbench tasks at pruning rates  $r \in \{50\%, 60\%, 70\%, 80\%\}$ . Tab. 2 summarizes the task success rate (SR), end-to-end speedup, and per-modality pruning rate (2D/3D PR).

**Comparison with MLA baseline.** Without any pruning, MLA achieves an average SR of 48.8% at 1.00× speed. Our framework at  $r=50\%$  delivers 47.5% SR (−1.3%) with a 2.49× speedup, and even at  $r=70\%$  the SR remains 46.3% (−2.5%) with 2.55× speedup, demonstrating that our method effectively prunes more than half of the visual tokens while preserving task performance.

**Comparison with baselines.** Naive Prune treats all tokens uniformly, incurring severe SR degradation (e.g., 6.7% on Close Box at  $r=50\%$ , −48.3% from baseline), whereas our method achieves 70.0% on the same task. SP-VLA [18] and VLA-Pruner [20], designed for SVLA models, fail to account for 2D/3D modality saliency differences when adapted to the MVLA setting. At  $r=60\%$ , SP-VLA obtains only 16.7% SR on Close Box with 1.37× speedup, while our method achieves 60.0% SR with 2.45× speedup. The key difference lies in modality-aware allocation: our framework adaptively assigns different pruning rates to 2D (e.g., 45.1%) and 3D (e.g., 72.8%) tokens, guided by modality saliency analysis.

**Speed advantage.** Our method consistently achieves 2.30×~2.69× speedup across all configurations, substantially outperforming baselines (1.21×~1.57×), because the tri-stage design leverages EMA to skip redundant computations across consecutive frames.

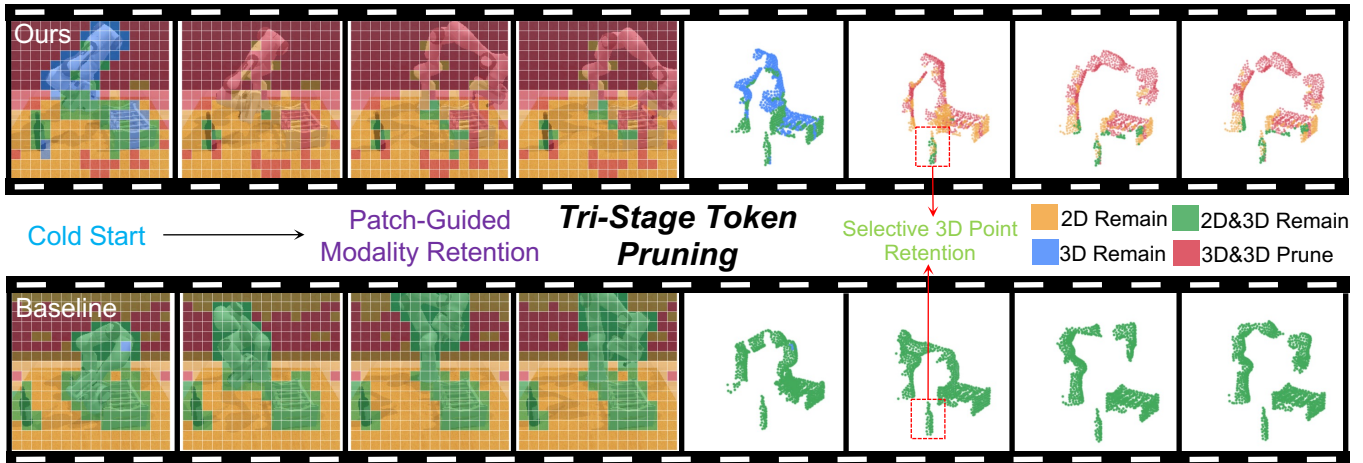


Figure 5: Results on Simulation Benchmark

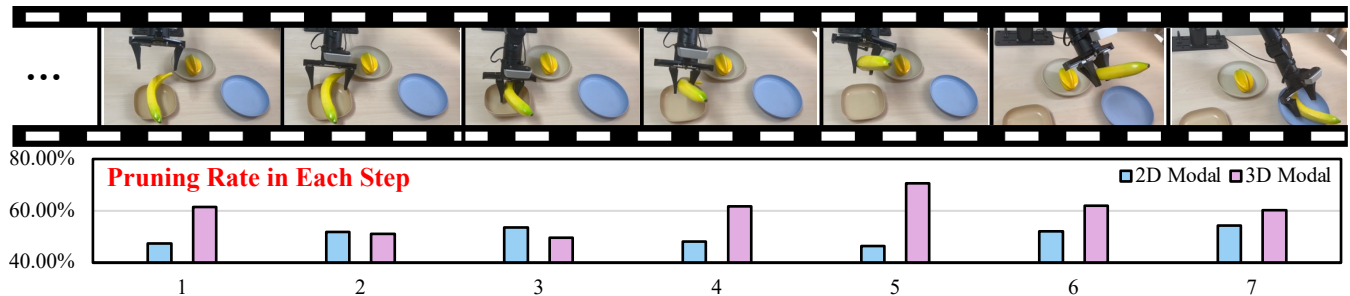


Figure 6: Results on Real-World Scenarios (Task Description: Pick up the Banana and Put it on the Blue Plate)

Table 3: Results of Ablation Study

Variants	S1	S2	S3	Average	
				SR	Speed
Baseline	-	-	-	70.0%	1.00×
+ Stage 1	✓	-	-	69.6%	1.22×
+ Stage 2	-	✓	-	69.8%	1.34×
+ Stage 1 + Stage 3	✓	-	✓	62.2%	1.35×
+ Stage 2 + Stage 3	-	✓	✓	71.5%	1.84×
+ Stage 1 + Stage 2	✓	✓	-	71.1%	1.55×
+ Stage 1 + Stage 2 + Stage 3	✓	✓	✓	70.0%	2.49×

**5.2.2 Results on Real-World Tasks.** Meanwhile, we conducted experiments on real-world tasks for our tri-stage token pruning strategy. We carried out various experiments on the Songling Piper robotic arm, monitoring the 2D/3D token pruning rate, the time consumption of each component, and the task success rate during the experiments. As an example, in Fig. 6, during the entire task process, the 2D token pruning rate was generally higher than the 3D one, and during the key interaction stage, the 3D token pruning rate showed a significant decrease, which is consistent with the analysis in Section 3. The average speedup ratio under different tasks reached 2.3 ×, and the task SR was reduced by less than 5%.

### 5.3 Ablation Study

To isolate the contribution of each stage, we conduct ablation studies by progressively enabling Stage 1 (S1, data preprocessing), Stage 2 (S2, semantic synthesis), and Stage 3 (S3, action iteration). Tab. 3 summarizes the results.

**Effect of individual stages.** Enabling Stage 1 alone (+ Stage 1) yields a 1.22× speedup with only −0.4% SR loss, confirming that the dual-threshold mechanism effectively prunes modality-redundant tokens. Enabling Stage 2 alone (+ Stage 2) achieves a larger 1.34× speedup with even less SR loss (−0.2%), as semantic-aware pruning removes background tokens without affecting task-critical regions.

**Effect of stage combinations.** Combining Stage 1 and Stage 2 yields 1.55× speedup and 71.1% SR—slightly above the baseline—demonstrating the complementarity between modality-level and spatial pruning. The full framework (+ Stage 1 + Stage 2 + Stage 3) further pushes the speedup to 2.49× while maintaining 70.0% SR, identical to the baseline. This significant acceleration gain from Stage 3 stems from the EMA prediction mechanism that avoids redundant per-frame computation.

**Importance of semantic guidance.** Notably, combining Stage 1 with Stage 3 without Stage 2 degrades SR to 62.2%, as temporal smoothing may propagate pruning errors without semantic-aware protection of task-critical tokens. In contrast, Stage 2 + Stage 3 achieves the highest SR of 71.5% with 1.84× speedup, validating that semantic context is essential for guiding temporal adaptation.

### 5.4 Discussion

**Overhead.** Tab. 4 reports per-step latency alongside each stage’s own method cost. All three pruning mechanisms introduce modest overhead (11–38 ms) yet yield substantial latency reductions, confirming that the token and frame savings far outweigh the added

**Table 4: Discussion of Overhead**

Variant	Method Cost	Latency (s)	Speedup
Baseline (MLA)	–	2.533	1.00×
+ Stage 1	12 ms	2.076	1.22×
+ Stage 2	38 ms	1.890	1.34×
+ Stage 3	11 ms	1.100	2.30×
Full (S1+S2+S3)	61 ms	<b>1.050</b>	<b>2.41×</b>

computation. The full framework totals 61 ms of method cost while achieving 2.41× speedup.

**Hyper-Parameters.** Our Tri-Stage framework involves four key hyper-parameters:  $\tau_{2D}$  and  $\tau_{3D}$  (dual thresholds in Stage 1), EMA momentum  $\beta$ , and sliding window size  $k$  (both in Stage 3). We sweep each on the Close Box task with the others fixed at defaults and report the results in Fig. 6. As shown, SR varies by less than 3.3% and speedup remains above 2.3× across all configurations, indicating that our framework is robust to hyper-parameter choices within reasonable ranges. We select  $\tau_{2D}=0.08$ ,  $\tau_{3D}=0.20$ ,  $\beta=0.85$ , and  $k=7$  as the defaults for all other experiments.

## 6 Conclusion

In this paper, we develop a tri-stage analysis for MVLA models, revealing the discrepancies and dynamics of 2D/3D modality saliency. Then we propose a corresponding tri-stage token pruning framework, to achieve optimal 2D/3D token pruning. Experiment show that, our framework achieves 2.55× speedup with minimal accuracy loss, while only cost 5.8% overhead.

## References

- [1] Rokas Bendikis, Daniel Dijkman, Markus Peschl, Sanjay Haresh, and Pietro Mazzaglia. 2025. Focusing on What Matters: Object-Agent-centric Tokenization for Vision Language Action models. arXiv:2509.23655 [cs.RO] <https://arxiv.org/abs/2509.23655>
- [2] Kevin Black, Noah Brown, Danny Driess, Adnan Esmail, Michael Equi, Chelsea Finn, Niccolo Fusai, Lachy Groom, Karol Hausman, Brian Ichter, et al. 2024.  $\pi_0$ : A Vision-Language-Action Flow Model for General Robot Control. arXiv preprint arXiv:2410.24164.
- [3] Anthony Brohan, Noah Brown, Justice Carbajal, Yevgen Chebotar, Xi Chen, Krzysztof Choromanski, Tianli Ding, Danny Driess, Avinava Dubey, Chelsea Finn, et al. 2024. Rt-2: Vision-language-action models transfer web knowledge to robotic control, 2023. URL <https://arxiv.org/abs/2307.15818> (2024), 2.
- [4] Anthony Brohan, Noah Brown, Justice Carbajal, Yevgen Chebotar, Joseph Dabis, Chelsea Finn, Keerthana Gopalakrishnan, Karol Hausman, Alex Herzog, Jasmine Hsu, et al. 2022. Rt-1: Robotics transformer for real-world control at scale. arXiv preprint arXiv:2212.06817.
- [5] Paweł Budzianowski, Wesley Maa, Matthew Freed, Jingxiang Mo, Winston Hsiao, Aaron Xie, Tomasz Młoduchowski, Viraj Tipnis, and Benjamin Bolte. 2025. Edgevla: Efficient vision-language-action models. arXiv preprint arXiv:2507.14049.
- [6] Liang Chen, Haozhe Li, Jiachen Li, et al. 2024. FastV: A Plug-and-Play Strategy to Accelerate Large Vision-Language Models. In *Proceedings of the IEEE/CVF Conference on Computer Vision and Pattern Recognition (CVPR)*. 2345–2355.
- [7] Alexey Dosovitskiy, Lucas Beyer, Alexander Kolesnikov, Dirk Weissenborn, Xiaohua Zhai, Thomas Unterthiner, Mostafa Dehghani, Matthias Minderer, Georg Heigold, Sylvain Gelly, et al. 2020. An image is worth 16x16 words: Transformers for image recognition at scale. arXiv preprint arXiv:2010.11929 (2020).
- [8] Danny Driess, Fei Xia, Mehdi SM Sajjadi, Corey Lynch, Aakanksha Chowdhery, Brian Ichter, Ayzan Wahid, Jonathan Tompson, Quan Vuong, Tianhe Yu, et al. 2023. Palm-e: An embodied multimodal language model. arXiv preprint arXiv:2303.03378.
- [9] Xianzhe Fan, Shengliang Deng, Xiaoyang Wu, Yuxiang Lu, Zhuoling Li, Mi Yan, Yujia Zhang, Zhizheng Zhang, He Wang, and Hengshuang Zhao. 2026. Any3D-VLA: Enhancing VLA Robustness via Diverse Point Clouds. arXiv preprint arXiv:2602.00807.
- [10] Saurabh Goyal, Anamitra Roy Choudhury, Saurabh Raje, Venkatesan Chakravarthy, Yogish Sabharwal, and Ashish Verma. 2020. Power-bert: Accelerating bert inference via progressive word-vector elimination. In *International conference on machine learning*. PMLR, 3690–3699.
- [11] Stephen James, Marc Freese, and Andrew J Davison. 2019. Pyrep: Bringing v-rep to deep robot learning. arXiv preprint arXiv:1906.11176 (2019).
- [12] Stephen James, Zicong Ma, David Rovick Arrojo, and Andrew J Davison. 2020. Rlbench: The robot learning benchmark & learning environment. *IEEE Robotics and Automation Letters* 5, 2 (2020), 3019–3026.
- [13] Huiqiang Jiang, Qianhui Wu, Chin-Yew Lin, Yuqing Yang, and Lili Qiu. 2023. LlmLingua: Compressing prompts for accelerated inference of large language models. In *Proceedings of the 2023 conference on empirical methods in natural language processing*. 13358–13376.
- [14] Titong Jiang, Xuefeng Jiang, Yuan Ma, Xin Wen, Bailin Li, Kun Zhan, Peng Jia, Yahui Liu, Sheng Sun, and Xianpeng Lang. 2025. The better you learn, the smarter you prune: Towards efficient vision-language-action models via differentiable token pruning. arXiv preprint arXiv:2509.12594 (2025).
- [15] Moo Jin Kim, Karl Pertsch, Siddharth Karamcheti, Ted Xiao, Ashwin Balakrishna, Suraj Nair, Rafael Rafailov, Ethan Foster, Grace Lam, Pannag Sanketi, et al. 2024. Openvla: An open-source vision-language-action model. arXiv preprint arXiv:2406.09246 (2024).
- [16] Chengmeng Li, Junjie Wen, Yaxin Peng, Yan Peng, and Yichen Zhu. 2026. Pointvla: Injecting the 3d world into vision-language-action models. *IEEE Robotics and Automation Letters* 11, 3 (2026), 2506–2513.
- [17] Xiaoqi Li, Liang Heng, Jiaming Liu, Yan Shen, Chenyang Gu, Zhuoyang Liu, Hao Chen, Nuowei Han, Renrui Zhang, Hao Tang, et al. 2025. 3ds-vla: A 3d spatial-aware vision language action model for robust multi-task manipulation. In *9th Annual Conference on Robot Learning*.
- [18] Ye Li, Yuan Meng, Zewen Sun, Kangye Ji, Chen Tang, Jiajun Fan, Xinzhu Ma, Shutao Xia, Zhi Wang, and Wenwu Zhu. 2025. Sp-vla: A joint model scheduling and token pruning approach for vla model acceleration. arXiv preprint arXiv:2506.12723 (2025).
- [19] Zhixuan Liang, Yizhuo Li, Tianshuo Yang, Chengyue Wu, Sitong Mao, Tian Nian, Liiao Pei, Shunbo Zhou, Xiaokang Yang, Jiangmiao Pang, et al. 2025. Discrete diffusion VLA: Bringing discrete diffusion to action decoding in vision-language-action policies. arXiv preprint arXiv:2508.20072 (2025).
- [20] Ziyang Liu, Yeqiu Chen, Hongyi Cai, Tao Lin, Shuo Yang, Zheng Liu, and Bo Zhao. 2025. VLA-Pruner: Temporal-Aware Dual-Level Visual Token Pruning for Efficient Vision-Language-Action Inference. arXiv preprint arXiv:2511.16449 (2025).
- [21] Zhuoyang Liu, Jiaming Liu, Jiadong Xu, Nuowei Han, Chenyang Gu, Hao Chen, Kaichen Zhou, Renrui Zhang, Kai Chin Hsieh, Kun Wu, et al. 2025. Mla: A multi-sensory language-action model for multimodal understanding and forecasting in robotic manipulation. arXiv preprint arXiv:2509.26642 (2025).
- [22] Ping Lu, Wenzhe Shi, and Xiuquan Qiao. 2024. Multi-View Image-Based 3D Reconstruction in Indoor Scenes: A Survey. *ZTE Communications* (10 2024).
- [23] Yunchao Ma, Yizhuang Zhou, Yunhuan Yang, Tiancai Wang, and Haoqiang Fan. 2025. Running VLAs at Real-time Speed. arXiv:2510.26742 [cs.RO] <https://arxiv.org/abs/2510.26742>
- [24] Ilija Radosavovic, Tete Xiao, Stephen James, Pieter Abbeel, Jitendra Malik, and Trevor Darrell. 2023. Real-world robot learning with masked visual pre-training. In *Conference on Robot Learning*. PMLR, 416–426.
- [25] Yongming Rao, Wenliang Zhao, Benlin Liu, Jiwen Lu, Jie Zhou, and Cho-Jui Hsieh. 2021. Dynamicvit: Efficient vision transformers with dynamic token sparsification. *Advances in neural information processing systems* 34 (2021), 13937–13949.
- [26] Mustafa Shukor, Dana Aubakirova, Francesco Capuano, Pepijn Kooijmans, Steven Palma, Adil Zouitine, Michel Aractingi, Caroline Pascal, Martino Russi, Andres Marafioti, et al. 2025. Smolvla: A vision-language-action model for affordable and efficient robotics. arXiv preprint arXiv:2506.01844 (2025).
- [27] Huifang Sun, Ge Li, Siheng Chen, Li Li, and Wei Gao. 2023. Editorial: 3D Point Cloud Processing and Applications. *ZTE Communications* (12 2023).
- [28] Xudong Tan, Yaoxin Yang, Peng Ye, Jialin Zheng, Bizhe Bai, Xinyi Wang, Jia Hao, and Tao Chen. 2025. Think twice, act once: Token-aware compression and action reuse for efficient inference in vision-language-action models. arXiv preprint arXiv:2505.21200 (2025).
- [29] Chongchong Wang, Yao Li, Beibei Wang, Hong Cao, and Yangyong Zhang. 2023. Point Cloud Processing Methods for 3D Point Cloud Detection Tasks. *ZTE Communications* (12 2023). <https://www.zte.com.cn/global/about/magazine/zte-communications/2023/en202304/special-topic/en202304005.html>
- [30] Hanzhen Wang, Jiaming Xu, Yushun Xiang, Jiayi Pan, Yongkang Zhou, Yong-Lu Li, and Guohao Dai. 2025. Specprune-vla: Accelerating vision-language-action models via action-aware self-speculative pruning. arXiv preprint arXiv:2509.05614 (2025).
- [31] Songsheng Wang, Rucheng Yu, Zhihang Yuan, Chao Yu, Feng Gao, Yu Wang, and Derek F Wong. 2025. Spec-vla: speculative decoding for vision-language-action models with relaxed acceptance. In *Proceedings of the 2025 Conference on Empirical Methods in Natural Language Processing*. 26916–26928.

- [32] Junjie Wen, Minjie Zhu, Yichen Zhu, Zhibin Tang, Jinming Li, Zhongyi Zhou, Chengmeng Li, Xiaoyu Liu, Yaxin Peng, Chaomin Shen, et al. 2024. Diffusion-vla: Generalizable and interpretable robot foundation model via self-generated reasoning. *arXiv preprint arXiv:2412.03293* (2024).
- [33] Siyu Xu, Yunke Wang, Chenghao Xia, Dihao Zhu, Tao Huang, and Chang Xu. 2025. VLA-Cache: Efficient Vision-Language-Action Manipulation via Adaptive Token Caching. *arXiv preprint arXiv:2502.02175* (2025).
- [34] Yuhao Xu, Yantai Yang, Zhenyang Fan, Yufan Liu, Yuming Li, Bing Li, and Zhipeng Zhang. 2026. QVLA: Not All Channels Are Equal in Vision-Language-Action Model’s Quantization. *arXiv preprint arXiv:2602.03782* (2026).
- [35] Cheng Yang, Yang Sui, Jinqi Xiao, Lingyi Huang, Yu Gong, Chendi Li, Jinghua Yan, Yu Bai, Ponnuswamy Sadayappan, Xia Hu, et al. 2025. Topv: Compatible token pruning with inference time optimization for fast and low-memory multimodal vision language model. In *Proceedings of the Computer Vision and Pattern Recognition Conference*. 19803–19813.
- [36] Yantai Yang, Yuhao Wang, Zichen Wen, Luo Zhongwei, Chang Zou, Zhipeng Zhang, Chuan Wen, and Linfeng Zhang. 2025. Efficientvla: Training-free acceleration and compression for vision-language-action models. *arXiv preprint arXiv:2506.10100* (2025).
- [37] Zhenyu Zhang, Ying Sheng, Tianyi Zhou, Tianlong Chen, Lianmin Zheng, Ruisi Cai, Zhao Song, Yuandong Tian, Christopher Ré, Clark Barrett, et al. 2023. H2o: Heavy-hitter oracle for efficient generative inference of large language models. *Advances in Neural Information Processing Systems* 36 (2023), 34661–34710.
- [38] Meng Zhao, Zhen Lin, et al. 2023. Roboflamingo: Providing a novel framework for vision-language-action models. *arXiv preprint arXiv:2311.01378* (2023).
- [39] Haoyu Zhen, Xiaowen Qiu, Peihao Chen, Jincheng Yang, Xin Yan, Yilun Du, Yin-Hong, and Chuang Gan. 2024. 3d-vla: A 3d vision-language-action generative world model. *arXiv preprint arXiv:2403.09631* (2024).
- [40] Zihao Zheng, Hangyu Cao, Jiayu Chen, Sicheng Tian, Chenyue Li, Maoliang Li, Xinhao Sun, Guojie Luo, and Xiang Chen. 2026. RoboECC: Multi-Factor-Aware Edge-Cloud Collaborative Deployment for VLA Models. arXiv:2603.20711 [cs.DC] <https://arxiv.org/abs/2603.20711>
- [41] Zihao Zheng, Hangyu Cao, Sicheng Tian, Jiayu Chen, Maoliang Li, Xinhao Sun, Hailong Zou, Zhaobo Zhang, Xuanzhe Liu, Donggang Cao, Hong Mei, and Xiang Chen. 2026. DyQ-VLA: Temporal-Dynamic-Aware Quantization for Embodied Vision-Language-Action Models. arXiv:2603.07904 [cs.LG] <https://arxiv.org/abs/2603.07904>
- [42] Zihao Zheng, Zhihao Mao, Maoliang Li, Jiayu Chen, Xinhao Sun, Zhaobo Zhang, Donggang Cao, Hong Mei, and Xiang Chen. 2026. KERV: Kinematic-Rectified Speculative Decoding for Embodied VLA Models. arXiv:2603.01581 [cs.RO] <https://arxiv.org/abs/2603.01581>
- [43] Zihao Zheng, Zhihao Mao, Sicheng Tian, Maoliang Li, Jiayu Chen, Xinhao Sun, Zhaobo Zhang, Xuanzhe Liu, Donggang Cao, Hong Mei, et al. 2026. HeiSD: Hybrid Speculative Decoding for Embodied Vision-Language-Action Models with Kinematic Awareness. *arXiv preprint arXiv:2603.17573* (2026).
- [44] Zihao Zheng, Zhihao Mao, Xingyue Zhou, Jiayu Chen, Maoliang Li, Xinhao Sun, Hailong Zou, Zhaobo Zhang, Xuanzhe Liu, Donggang Cao, et al. 2026. VLN-Cache: Enabling Token Caching for VLN Models with Visual/Semantic Dynamics Awareness. *arXiv preprint arXiv:2603.07080* (2026).
- [45] Zihao Zheng, Sicheng Tian, Hangyu Cao, Chenyue Li, Jiayu Chen, Maoliang Li, Xinhao Sun, Hailong Zou, Guojie Luo, and Xiang Chen. 2026. RAPID: Redundancy-Aware and Compatibility-Optimal Edge-Cloud Partitioned Inference for Diverse VLA Models. arXiv:2603.07949 [cs.DC] <https://arxiv.org/abs/2603.07949>
- [46] Y Zhu et al. 2023. Vima: General robot manipulation with multimodal prompts. In *International Conference on Learning Representations (ICLR)*.

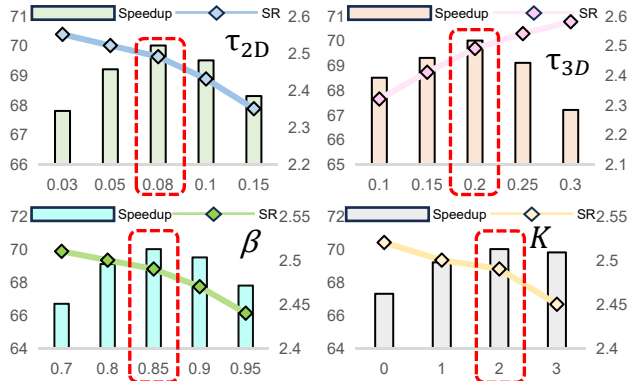


Figure 7: Hyperparameters Selection

## A Discussion on Hyperparameters

Our Tri-Stage token pruning framework introduces four key hyperparameters: the dual thresholds  $\tau_{2D}$  and  $\tau_{3D}$  in the data preprocessing stage, alongside the Exponential Moving Average (EMA) momentum  $\beta$  and the sliding window size  $k$  in the action iteration stage. To systematically evaluate their impacts on the trade-off between task success rate (SR) and inference speedup, we conduct parameter sweeps on the Close Box task, as illustrated in Fig. 7. During the evaluation of each specific parameter, the others are fixed at their empirically optimal default values ( $\tau_{2D} = 0.08$ ,  $\tau_{3D} = 0.20$ , and  $\beta = 0.85$ ).

As shown in the trends,  $\tau_{2D}$  and  $\tau_{3D}$  directly control the aggressiveness of the modality-level coarse filtering. Increasing  $\tau_{2D}$  or decreasing  $\tau_{3D}$  expands the dual-retention candidate set, which inherently preserves more tokens and slightly reduces the speedup. Conversely, overly aggressive thresholds risk discarding critical 2D texture or 3D geometric features, leading to noticeable SR degradation. Meanwhile,  $\beta$  and  $k$  govern the temporal stability of the pruning decisions. A smaller  $\beta$  makes the mask predictions overly sensitive to instantaneous inter-frame mutations, while an excessively large  $\beta$  causes the temporal smoothing to lag behind actual physical dynamics, both of which negatively impact the control precision. Overall, the SR varies within a narrow margin and the speedup remains consistently high (above 2.3 $\times$ ) across a wide range of configurations, demonstrating that our framework is highly robust to hyperparameter choices.

## B Tri-Stage Token Pruning Details

To intuitively demonstrate the internal mechanics of our framework, we visualize the step-by-step token pruning process in Fig. 8. We select the Take Umbrella out of Umbrella Stand task as a representative example to illustrate the dynamic evolution of the retention masks across consecutive steps. The color-coding indicates the pruning decisions for each patch: Light Blue represents retaining 2D tokens only, Light Green indicates retaining both 2D and 3D modalities, and Gray means neither is retained (pruned).

### B.1 Stage 1: Data Preprocessing

As illustrated in the first row of Fig. 8, Stage 1 implements the conclusion derived from insight ①, where the  $L_1$  norm of 2D and 3D features is utilized to roughly delineate key interaction regions and

isolate them from the background. While this mechanism successfully highlights feature-rich regions (such as the target bounding box, marked by the green “Key Interaction” bounding box), it still retains a significant number of task-irrelevant background tokens. This visually confirms that although low-level feature norms can capture basic modal saliency, they lack a holistic semantic understanding of the scene, resulting in a coarse and noisy initial filtering process that necessitates further refinement in subsequent stages.

### B.2 Stage 2: Semantic Synthesis

The second row of Fig. 8 visualizes the impact of introducing semantic synthesis candidate selection. By categorizing the scene into distinct semantic sets (target, robot, and background) using attention scores, our framework accurately identifies and discards irrelevant regions. The red bounding box and arrow, labeled “Semantic Synthesis Candidate Selection,” explicitly highlight how the scattered, noisy background patches from Stage 1 are uniformly pruned (turning gray). Concurrently, the critical spatial features within the key interaction region are strictly protected. This intersection of local features and global semantics ensures a highly structured and cohesive retention mask.

### B.3 Stage 3: Action Iteration

Robotic manipulation is inherently dynamic. Relying solely on instantaneous, per-frame calculations can lead to inter-frame flickering and unstable pruning boundaries, which disrupts continuous control. The third row of Fig. 8 illustrates the effect of our temporal dynamics analysis. By applying an Exponential Moving Average (EMA) mechanism over a sliding window, the temporally smoothed predictions prevent abrupt mutations in the mask. As indicated by the yellow bounding boxes connected by the “Stable Action Iteration” curve, the candidate sets transition gradually and naturally as the robotic arm. This predictive stabilization prevents feature disruption during critical manipulation phases, directly contributing to the high task success rate observed in our experiments.

## C MVLA Models

Multi-Visual-Modal Vision-Language-Action (MVLA) models extend VLA architectures by incorporating 3D spatial modalities to map multi-sensory observations and natural language instructions directly to robot actions, as illustrated in Fig. 9. The common MVLA architecture generally follows a three-stage pipeline: (1) data tokenization, where specialized 2D and 3D encoders process the input image and point cloud to generate 2D and 3D visual tokens, while a text tokenizer processes the language instruction; (2) semantic synthesis, where a pre-trained Large Language Model (LLM) backbone fuses these concatenated multimodal tokens for cross-modal reasoning; and (3) action decoding, where the model outputs are processed by an action detokenizer to yield a precise action slice for subsequent robot execution.

Formally, at a given timestep  $t$ , the MVLA model receives a natural language instruction  $L$ , a 2D observation  $I_t$ , and a 3D observation  $P_t$ . During the data preprocessing stage, the visual encoders project these raw inputs into token sequences. These 2D and 3D embeddings are then concatenated with the language tokens  $E_L$  and fed into the LLM backbone to perform semantic reasoning

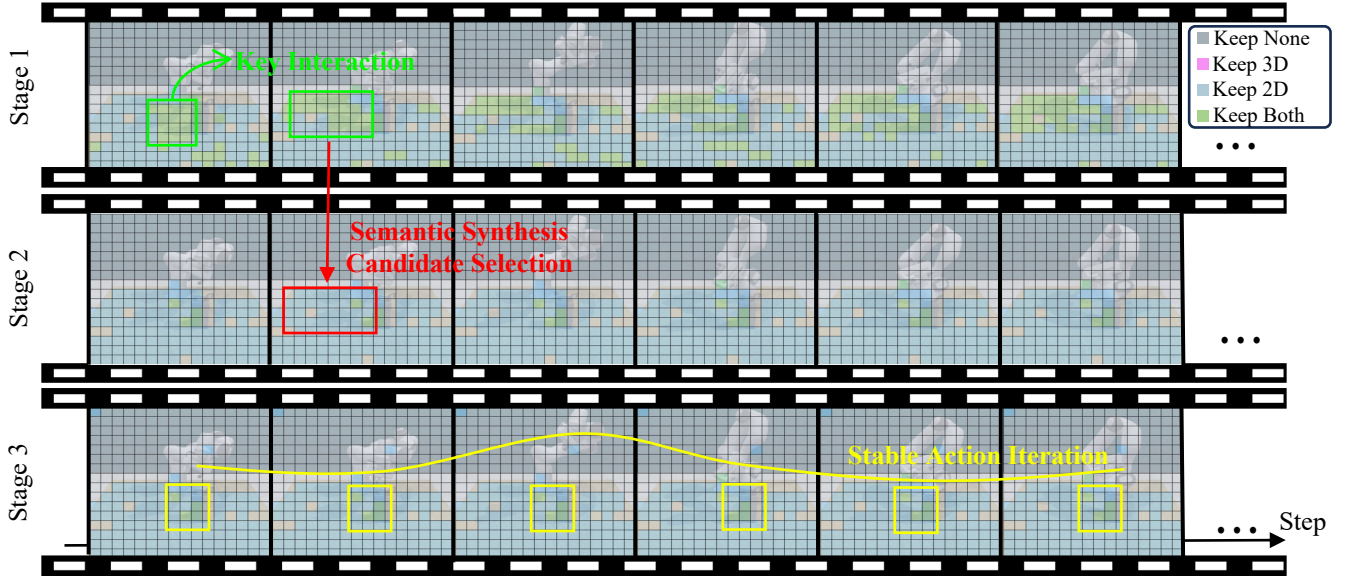


Figure 8: Tri-Stage Candidate Selection Visualization (Task Description: Take Umbrella out of Umbrella Stand)

and generate the hidden states  $H_t$ . Finally, an action decoder maps the hidden states  $H_t$  into precise robot control signals  $A_t$  (e.g., 7-DoF end-effector poses). While this modal expansion from 2D-only to 2D+3D significantly improves spatial perception, it natively introduces a massive increase in sequence length and 2D/3D token redundancy, which our tri-stage pruning framework aims to optimize.

To illustrate this architecture concretely, we adopt the MLA [21] as our baseline, which represents a state-of-the-art MVLA model. Specifically, MLA utilizes a LLaMA-2 7B backbone and employs lightweight tokenizers to project 2D images and 3D point clouds into  $N_{img} = 256$  and  $N_{pc} = 256$  tokens, respectively. After processing the concatenated tokens, a diffusion-based action decoder is employed to autoregressively denoise and predict the continuous robot actions.

## D Dataset and Simulation Benchmark

To systematically evaluate the performance of our token pruning framework, we conduct simulation experiments on the RL Bench benchmark [12]. RL Bench is a large-scale robot learning environment built upon the CoppeliaSim physics engine, providing a rich set of everyday manipulation tasks with high-quality demonstration trajectories.

Based on the capabilities of the MVLA model, we select five representative and contact-rich tasks that require rigorous spatial perception and precise manipulation: Close Box, Close Fridge, Close Laptop, Sweep to Dustpan, and Phone on Base. Each task presents unique geometric challenges. For instance, Close Laptop and Close Box demand accurate 3D spatial positioning to avoid collisions, while Sweep to Dustpan requires continuous trajectory adjustments based on 2D/3D visual feedback. During the evaluation, each task is evaluated over 30 trials with randomized initial states (e.g., varying object poses and positions) to ensure the robustness of the success rate (SR) measurements.

## E Real-World Environment and Tasks

To validate the effectiveness of our framework in physical environments, we construct a real-world tabletop manipulation setup. 1) Hardware Configuration: We employ a 7-DoF Songling Piper (AgileX PIPER) robotic arm equipped with a parallel gripper as the end-effector. For multisensory observation, the setup mimics the dual-view configuration common in MVLA frameworks. We utilize RGB-D cameras deployed at two specific viewpoints: a third-person camera fixed in front of the tabletop to capture the global workspace overview, and a wrist-mounted camera attached to the robotic arm to provide fine-grained, object-centric visual and geometric feedback during interactions. 2) Task Environment: The experiments are conducted on a standardized tabletop workspace. We design multiple manipulation tasks, such as grasping and spatial displacement of household objects (e.g., picking up target items and placing them into designated containers). The physical environment introduces natural variations in lighting, background clutter, and object textures, which comprehensively tests the pruning framework’s capability to retain salient 2D and 3D tokens under real-world noise.

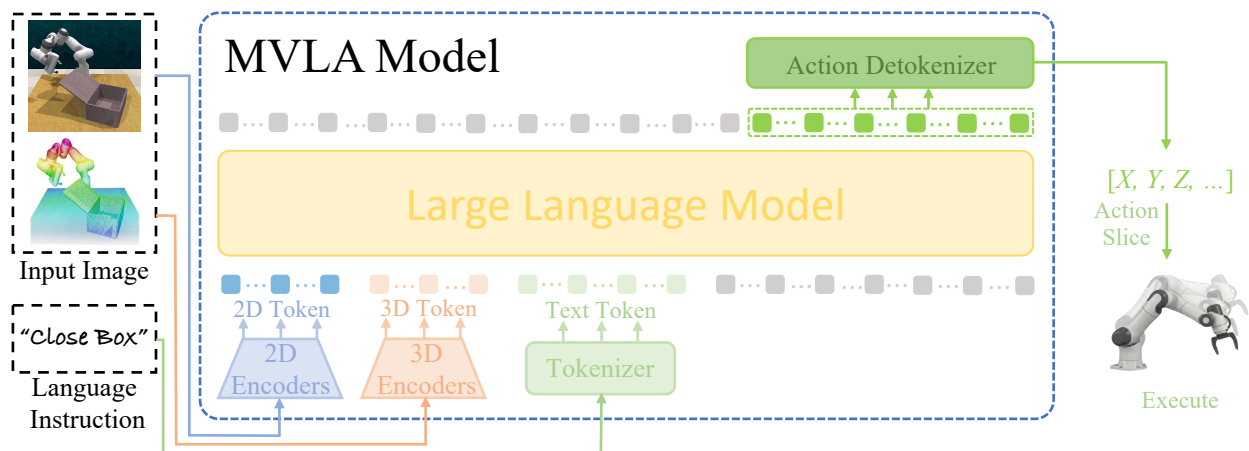


Figure 9: Common Structure of Multi-Visual-Modal VLA (MVLA) Models